LETTERS

Observation of spin Coulomb drag in a two-dimensional electron gas

C. P. Weber[1], N. Gedik[1,2], J. E. Moore[1], J. Orenstein[1], J. Stephens[3] & D. D. Awschalom[3]

An electron propagating through a solid carries spin angular momentum in addition to its mass and charge. Of late there has been considerable interest in developing electronic devices based on the transport of spin that offer potential advantages in dissipation, size and speed over charge-based devices[1]. However, these advantages bring with them additional complexity. Because each electron carries a single, fixed value ($-e$) of charge, the electrical current carried by a gas of electrons is simply proportional to its total momentum. A fundamental consequence is that the charge current is not affected by interactions that conserve total momentum, notably collisions among the electrons themselves[2]. In contrast, the electron's spin along a given spatial direction can take on two values, $\pm\hbar/2$ (conventionally $\uparrow, \downarrow$), so that the spin current and momentum need not be proportional. Although the transport of spin polarization is not protected by momentum conservation, it has been widely assumed that, like the charge current, spin current is unaffected by electron–electron (e–e) interactions. Here we demonstrate experimentally not only that this assumption is invalid, but also that over a broad range of temperature and electron density, the flow of spin polarization in a two-dimensional gas of electrons is controlled by the rate of e–e collisions.

In this work, spin diffusion is characterized by the transient spin grating technique[3], which is based on the optical injection of spin-polarized electrons. The two-dimensional electron gas (2DEG) resides in a GaAs quantum well, in which the carriers are donated by Si impurities doped into the GaAlAs barrier layers. Near-bandgap illumination of the GaAs excites electrons whose initial spin is determined by the helicity of the light[4]. If the GaAs is excited by two non-collinear, coherent beams of light with orthogonal linear polarization, then in the region where the beams interfere the helicity varies sinusoidally from plus one to minus one. The optical-helicity wave generates a wave of electron-spin polarization with the same spatial frequency, which in turn generates a sinusoidal variation (grating) in the index of refraction through the Kerr effect. The wavevector of the injected spin-density wave is in the plane of the 2DEG, and the spin polarization is oriented perpendicular to this plane.

The time evolution of the transient spin grating directly reveals the nature of spin transport and relaxation in the electronic system, functioning like a time-domain version of neutron scattering. We measure the spin polarization by detecting the diffraction of a probe beam off the grating. A sensitive coherent detection scheme (Methods) enabled acquisition of the ~150 grating decays required to characterize the spin dynamics for each sample throughout the temperature–wavevector (T–q) parameter space.

In this Letter we present results for three quantum well samples, with electron concentrations of 7.8×10^{11}, 4.3×10^{11} and $1.9 \times 10^{11}\,\mathrm{cm}^{-2}$, corresponding to Fermi temperatures of 400, 220 and 100 K, respectively. Figure 1 shows the initial decay rate of the spin grating as function of T in the most heavily doped sample, for several grating wavevectors from 0.4×10^4 to $2.5 \times 10^4\,\mathrm{cm}^{-1}$. The dependence on T can be described in terms of three regions. For $100\,\mathrm{K} < T < 300\,\mathrm{K}$, the decay rate varies slowly. For $50\,\mathrm{K} < T < 100\,\mathrm{K}$, the decay rate increases rapidly with decreasing T, and for $T < 50\,\mathrm{K}$, it reaches a slowly varying plateau.

We begin by discussing the decay rate where it varies slowly, that is, below 50 K and above 100 K. In the high-T region, the spin dynamics

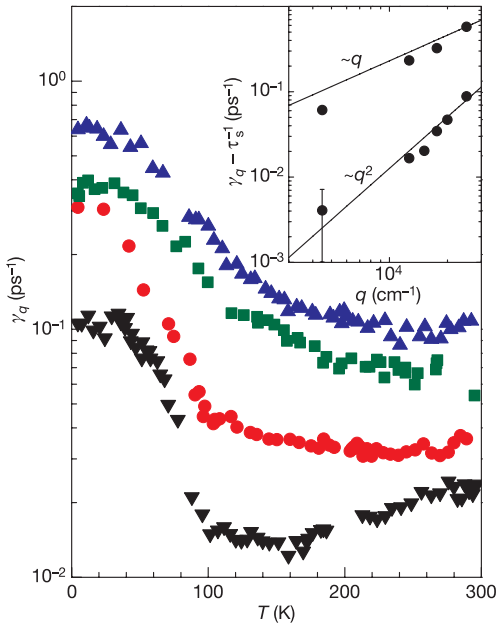

Figure 1 | Spin-grating decay at various wavevectors (q) and temperatures (T) for the sample with Fermi temperature 400 K. Main panel, the initial decay rate, γ_q, of the spin grating as a function of T for (bottom to top) $q = 0.45 \times 10^{-4}$, 1.3×10^{-4}, 1.8×10^{-4} and $2.5 \times 10^{-4}\,\mathrm{cm}^{-1}$. Inset, the initial decay rate of the spin grating as a function of q. Points are $\gamma_q - \tau_s^{-1}$; τ_s is obtained from decay of homogenous ($q = 0$) spin excitation. Error bars (s.d.) are the size of the points except as shown. Lower points and line, room temperature. The line is a fit of the data to $\gamma_q = \tau_s^{-1} + D_s q^2$, giving a spin diffusion length $L_s = (D_s\tau_s)^{1/2} = 0.81\,\mu\mathrm{m}$ and a 'spin mean-free-path' $l = 2D_s/v_F = 60\,\mathrm{nm}$. The observation of diffusive motion is internally consistent, as l is much smaller than both L_s and the smallest grating wavelength, 2.5 μm. Upper points and line, 5 K. The line has slope = 1, corresponding to ballistic, rather than diffusive, spin-motion with a velocity of $2.3 \times 10^7\,\mathrm{cm\,s}^{-1}$.

[1]Physics Department, University of California, Berkeley, and Materials Science Division, Lawrence Berkeley National Laboratory, Berkeley, California 94720, USA. [2]Laboratory for Molecular Sciences, Arthur Amos Noyes Laboratory of Chemical Physics, California Institute of Technology, Pasadena, California 91125, USA. [3]Center for Spintronics and Quantum Computation, University of California, Santa Barbara, California 93106, USA.

can be accurately described in terms of independent processes of spin diffusion and spin relaxation. In this description, the decay rate varies with q quadratically, as $\gamma_q = \tau_s^{-1} + D_s q^2$, where D_s is the spin diffusion coefficient and τ_s is the spin relaxation time[3]. In the inset to Fig. 1 we plot $\gamma_q - \tau_s^{-1}$ versus q at 295 K (lower points) and 5 K (upper points), on logarithmic axes. Here $1/\tau_s$ is independently determined from the decay rate of the circular dichroism induced by a circularly polarized pump beam[5] (see Supplementary Information). A comparison of the 295 K data with a line of slope two shows that the decay of the grating is well described by diffusive dynamics, with $D_s = 130\,\mathrm{cm^2\,s^{-1}}$ and $\tau_s = 50$ ps.

Next, we examine the spin-grating dynamics at $T < 50$ K. As shown in Fig. 1 inset, the initial decay rates at 5 K are linear in q at the higher wavevectors. The change in power law exponent from two to one indicates that a crossover from diffusive to ballistic dynamics takes place as the sample temperature is lowered. In the ballistic regime, electrons propagate a distance comparable to the grating wavelength, Λ, without scattering and the initial decay rate is $v_F q$, the reciprocal of the time required for an electron moving with the Fermi velocity (v_F) to traverse a distance $\Lambda/2\pi$.

Although the grating's initial decay rate saturates near $v_F q$ when T reaches ~50 K, its time dependence continues to change as T is lowered further. Figure 2 shows the grating amplitude as function of time for several temperatures between 5 K and 100 K, measured with a grating wavevector of $2.5 \times 10^4\,\mathrm{cm^{-1}}$ (the T indicated is the lattice temperature, which is below the electron temperature, as will be discussed later). An oscillatory structure appears in the decay curves, becoming increasingly pronounced as T decreases. The growth of these oscillations is a consequence of the increase of the mean-free-path, l, in the regime where $ql \geq 1$.

To determine D_s from data such as those in Fig. 2, we use an expression for the time dependence of a spin fluctuation that is applicable throughout the diffusive–ballistic crossover regime. If a spin polarization wave is introduced at $t = 0$, its subsequent time dependence is the Fourier transform of $S(q,\omega) \propto [i\omega - D(q,\omega)q^2]^{-1}$, where $D(q,\omega)$ is the dynamic spin diffusivity. In the limit $q \ll k_F$,

$$D(q,\omega) = \frac{v_F/2}{\sqrt{(i\omega/v_F - 1/l)^2 + q^2}} \qquad (1)$$

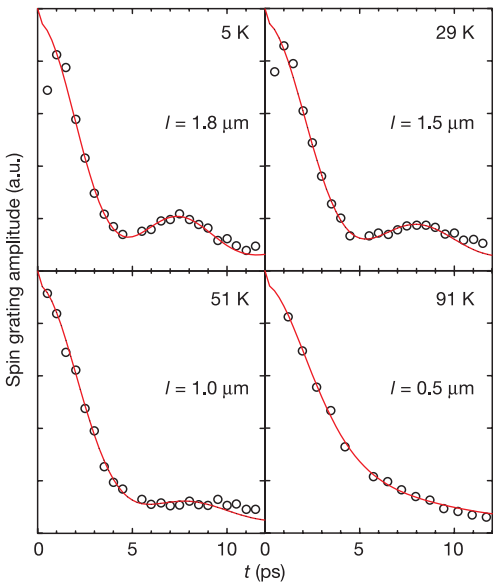

Figure 2 | Time dependence of the spin grating's amplitude. The lines are fits of the data to $S(q,\omega)$. The values of l determined from these fits are indicated in each panel. Owing to laser heating, the temperature T_e of the electron gas is higher than the lattice temperatures indicated.

where equation (1) extrapolates from the small-q limit[6] to the ballistic regime. In attempting to fit the grating decay curves in the plateau regime, we found that equation (1) is not quite sufficient to describe the data. It is necessary to add to the Fourier transform of $S(q,\omega)$ a small, slowly decaying exponential with relative initial amplitude ~0.1 and characteristic time ~25 ps. We speculate that this slow exponential may originate from a small fraction of localized electrons. The solid lines through the data points in Fig. 2 show the results of the fitting procedure, with fitting parameters l, v_F and the amplitude and time constant of the slow exponential. Despite the complicating presence of the slow exponential, we believe that the fits give an accurate indication of l, as this is the only parameter that determines the rate at which the oscillations are damped. Finally, the spin diffusion coefficient is determined from the relation $D_s = v_F l/2$.

The temperature dependence of D_s obtained from our analysis of the spin-grating dynamics is shown in Fig. 3 for quantum wells of different electron density. For the two lower-density samples (middle and lower panels), the dynamics were diffusive at all T, consistent with their lower mobility. To characterize charge transport in the same set of samples, we performed 4-probe measurements of the 2D charge conductance, σ_c, carrier density, n, and mobility, μ, on chips from the same set of wafers. Together, these measurements allow us to test the assumption that the scattering processes that control spin diffusion and charge conduction are the same. The link between conductance and diffusion coefficient is the Einstein relation, $D_s = \sigma_s/e^2\chi_s$, where σ_s and χ_s are the spin conductance and

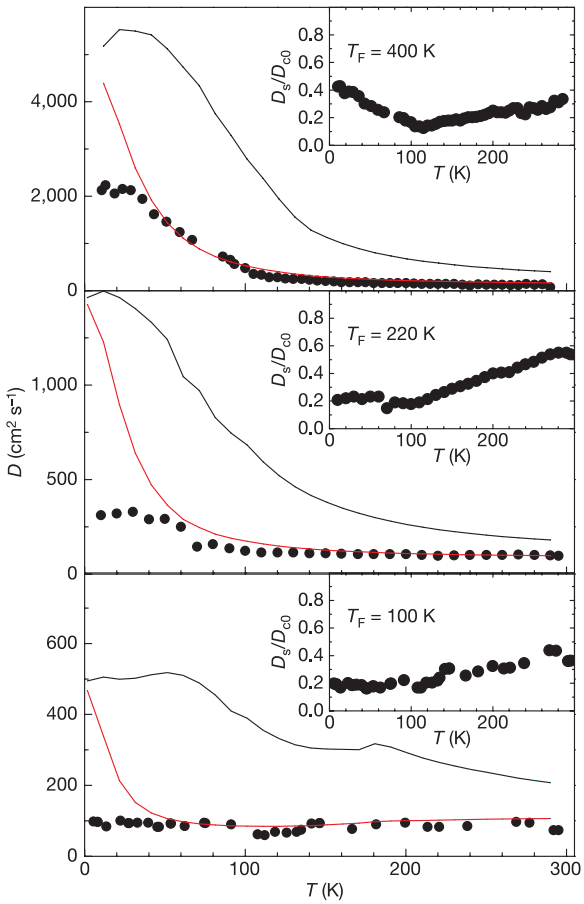

Figure 3 | Comparison of motion of spin and charge, for samples with the Fermi temperatures (T_F) shown. Dots (main panels), spin-diffusion coefficients D_s determined from optical measurements. Black lines, quasiparticle diffusion coefficients D_{c0} determined from transport data. Insets, D_s/D_{c0}. Red lines, D_s predicted from spin Coulomb drag theory, taking $\chi_s = \chi_0$.

susceptibility, respectively. If the spin and charge scattering rates were the same (that is, $\sigma_c = \sigma_s$), then D_s would equal $(\chi_0/\chi_s)D_{c0}$ (ref. 7), where $D_{c0} = \sigma_c/e^2\chi_0$ and $\chi_0 = N_F(1 - e^{-E_F/k_BT})$ is the non-interacting susceptibility (see Supplementary Information; E_F is the Fermi energy, N_F is the density of states at E_F, and k_B is Boltzmann's constant). Physically, D_{c0} is the quasiparticle diffusion coefficient[7], approaching $\mu E_F/e$ and $\mu k_B T/e$ in the degenerate and non-degenerate regimes, respectively. D_{c0} calculated from the 4-probe transport data and plotted in Fig. 3 is considerably larger than D_s at all T and for each of the samples. The ratio is far greater than can be accounted for by many-body enhancement of the spin susceptibility, as the factor χ_s/χ_0 is less than 1.4 in this range of electron density[8,9].

The contrast in the diffusion coefficients of charge and spin is surprising, as the assumption $D_s = D_{c0}$ is widely used in modelling spin transport in semiconductors. However, this assumption fails to take into account *e–e* collisions, whose rate can be much faster than those of impurity or phonon scattering. The *e–e* scattering events can be ignored in the description of charge transport because they conserve total momentum. However, they can have a profound effect on spin transport, as illustrated in Fig. 4. For the collision depicted between electrons with opposite spin, the charge current is conserved while the spin current reverses direction.

D'Amico and Vignale have proposed that the microscopic process shown in Fig 4 can change the nature of macroscopic spin transport. Seen macroscopically, *e–e* collisions transfer momentum between the spin-up and spin-down populations, creating a force damping their relative motion that these authors term 'spin Coulomb drag' (SCD)[10]. Spin diffusion, which requires a counterflow of the spin populations, is damped by SCD, while charge diffusion is not. (The recently observed[11,12] spin Hall effect also involves the counterflow of spin populations, and so should be damped by SCD.) According to D'Amico and Vignale[10], the reduction of D_s relative to D_{c0} is:

$$\frac{D_s}{D_{c0}} = \left(\frac{\chi_0}{\chi_s}\right)\frac{1}{1+|\rho_{\uparrow\downarrow}|/\rho} \qquad (2)$$

where $\rho = 1/\sigma_c$ is the charge resistance and $\rho_{\uparrow\downarrow}$ is the spin drag resistance, parameterizing the rate of momentum exchange between spin ↑ and ↓ electrons. D'Amico and Vignale, and Flensberg and Jensen[13], have calculated $\rho_{\uparrow\downarrow}(T)$ for a 2DEG using the random phase approximation, obtaining results that depend only on the electron density of the quantum well.

Equation (2) predicts that despite the complex T dependences of the individual diffusion coefficients, their ratio depends primarily on the single factor, $|\rho_{\uparrow\downarrow}|/\rho$. We test this prediction in Fig. 5, without invoking any assumptions or adjustable parameters, by plotting D_{c0}/D_s (the inverse of equation (2)) versus $|\rho_{\uparrow\downarrow}|/\rho$ for each of the three samples measured in this study. The transport coefficients are taken directly from our measurements, while $\rho_{\uparrow\downarrow}$ was calculated using equation (2) of ref. 14. The resulting graph reveals the simple linear dependence of D_{c0}/D_s on $|\rho_{\uparrow\downarrow}|/\rho$ predicted by equation (2) over a large range of $|\rho_{\uparrow\downarrow}|/\rho$, implying that SCD is indeed the origin of the large suppression of D_s relative to D_{c0}. The fact that the slope is slightly greater than unity is consistent with the expectation that the many-body enhancement of χ_s relative to χ_0 is small in this density regime[8,9]. Finally, the fact that D_{c0}/D_s extrapolates to near unity as $|\rho_{\uparrow\downarrow}|/\rho \rightarrow 0$ indicates that the spin and charge diffusion coefficients approach each other in the limit that the spin drag resistance becomes smaller than the ordinary resistance. This result provides independent evidence that the spin grating and four-probe techniques used in this work accurately measure equilibrium spin and charge transport coefficients, respectively.

Returning to the T dependence shown in Fig. 3, the solid lines show the prediction of equation (2) for D_s with the factor χ_0/χ_s set equal to unity. As could be anticipated from the discussion of Fig. 5, SCD quantitatively accounts for the suppression of D_s relative to D_{c0} over a broad range of temperature and electron density. It is clear, however, that the measured D_s consistently departs from theory below 40 K. We believe that this discrepancy indicates that at low T the photoexcited electron gas does not cool to the lattice temperature. If the electron gas retains the heat, Q, deposited by the excitation, its temperature T_e will rise to approximately $(T^2 + 2Q/\beta)^{1/2}$, where $\beta = 5.3 \times 10^5\,\mathrm{eV\,cm^{-2}\,K^{-2}}$ is the temperature coefficient of the electronic specific heat. We estimate $Q = 4.8 \times 10^8\,\mathrm{eV\,cm^{-2}}$, assuming that each absorbed photon deposits approximately 10 meV (the energy width of the laser pulse) into the Fermi sea. The resulting estimate for the minimum T_e is indeed $\sim$ 35 K.

Finally, we note that SCD can be highly advantageous for spintronic applications, as it increases the distance that a spin packet can be dragged by an electric field, E, before it spreads owing to diffusion[15]. The length L_D that a packet of width w will drift before it broadens by a factor of two is $w^2 e\mu/D_s$. In the absence of SCD, the ratio μ/D_s equals e/k_BT_F (where T_F is Fermi temperature) or e/k_BT in the degenerate or non-degenerate regimes, respectively, and L_D/w is independent of the underlying scattering rates. In the degenerate regime, for example, $L_D/w = eEw/k_BT_F$; drifting a spin packet farther than w is only possible in a strong E limit, where the potential drop across the packet exceeds the Fermi energy. Introducing SCD slows the counterflow of spin ↑ and ↓ electrons without affecting their co-propagation, amplifying L_D/w by the factor $1 + |\rho_{\uparrow\downarrow}(T)|/\rho$. Clean materials with strong *e–e* scattering will have the largest values

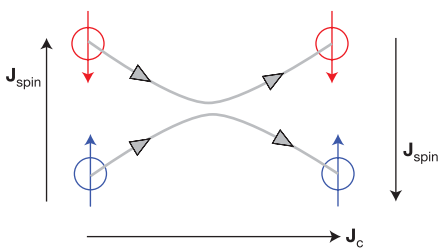

Figure 4 | A representation of *e–e* scattering that does not conserve spin-current. Before the collision the spin-current, J_{spin}, is positive; after, it is negative. The charge current, J_C, does not change. Colours correspond to spin states

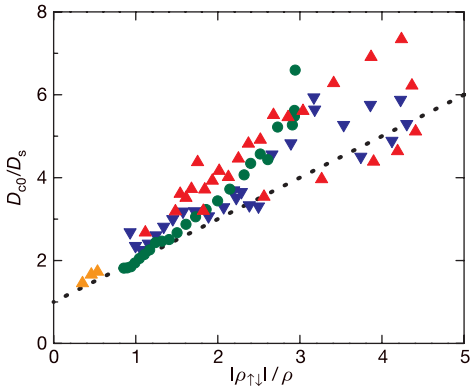

Figure 5 | Relation between suppression of spin diffusion and spin drag resistance. x-axis, ratio of $|\rho_{\uparrow\downarrow}(T)|$ (where $\rho_{\uparrow\downarrow}$ is the spin drag resistance), determined from SCD theory[14], to measured resistivity, ρ. y-axis, ratio of quasiparticle diffusion coefficient, D_{c0}, to spin diffusion coefficient, D_s. Temperature is an implicit parameter. Points are for samples with $T_F = 400$ K (red), 220 K (green) and 100 K (blue). Points for $T < 40$ K are not shown because the electrons do not cool below 40 K. Orange, points for a sample with $T_F = 400$ K, with ρ increased by depositing a portion of the Si dopants into the well. Line has unity slope and intercept, indicating the prediction of equation (2) for $\chi_s = \chi_0$. For points above the line, $\chi_s > \chi_0$.

of $|\rho_{\uparrow\downarrow}(T)|/\rho$, and hence be the best media for propagation of spin information.

METHODS

Quantum well characteristics. The GaAs/$Ga_{0.7}Al_{0.3}As$ samples were grown in the (100) direction by molecular beam epitaxy, and each consist of ten quantum wells of thickness 12 nm, separated by 48 nm barriers. The Si impurities were deposited in eight single atomic layers in the centre 14 nm of each barrier to maximize their distance from the 2DEG. The carrier concentration, n, mobility, μ, and electrical resistivity, ρ, were measured using 4-probe transport techniques without illumination. For the samples with n of 7.8×10^{11}, 4.3×10^{11} and 1.9×10^{11} cm^{-2} per quantum well, at low temperature μ reached 240,000, 92,000 and 69,000 $cm^2 V^{-1} s^{-1}$, respectively.

Optical methods. The two interfering beams that generate the optical-helicity wave derive from a Ti:sapphire laser, which produces a train of optical pulses with duration 100 fs, interpulse separation 11 ns and centre wavelength 820 nm. The incident power density for most measurements was $\sim$500 W cm^{-2}, corresponding to $\sim$6 W cm^{-2} absorbed per quantum well. For $T > 35$ K, grating decay rates did not change when measured at incident powers down to 100 W cm^{-2}, suggesting that photoinduced holes do not play a significant role in the electron spin transport (typical electron hole recombination times were $\sim$750 ps). At low T the grating decay rate increased slowly with decreasing power, consistent with the electron heating model described in the main text.

The grating wavevector was directed along the GaAs $(00\bar{1})$ direction. To detect the induced spin grating, we mixed diffracted and transmitted probes to produce a photodetector current linear in the diffracted field[16–18]. The decisive advantage in this scheme is realized by modulating the relative phase of these two beams sinusoidally at 1.2 kHz. Synchronous detection with a lock-in amplifier at the modulation frequency leads to considerable rejection of laser noise and stray light.

Received 29 April; accepted 2 September 2005.

1. Awschalom, D. D., Loss, D. & Samarth, N. (eds) *Semiconductor Spintronics and Quantum Computation* (Springer, Berlin, 2002).
2. Ziman, J. M. *Electrons and Phonons: The Theory of Transport Phenomena in Solids* (Oxford Univ. Press, New York, 2001).
3. Cameron, A. R., Riblet, P. & Miller, A. Spin gratings and the measurement of electron drift mobility in multiple quantum well semiconductors. *Phys. Rev. Lett.* **76,** 4793–4796 (1996).
4. Meier, F. & Zakharchenya, B. *Optical Orientation* (North-Holland, Amsterdam, 1984).
5. Bar-Ad, S. & Bar-Joseph, I. Exciton spin dynamics in GaAs heterostructures. *Phys. Rev. Lett.* **68,** 349–352 (1992).
6. Rammer, J. *Quantum Transport Theory* (Perseus Books, Reading, Massachusetts, 1998).
7. Castellani, C., DiCastro, C., Kotliar, G., Lee, P. A. & Strinati, G. Thermal conductivity in disordered interacting-electron systems. *Phys. Rev. Lett.* **59,** 477–480 (1987).
8. Yarlagadda, S. & Giuliani, G. F. Spin susceptibility in a two-dimensional electron gas. *Phys. Rev. B* **40,** 5432–5440 (1989).
9. Kwon, Y., Ceperley, D. M. & Martin, R. M. Quantum Monte Carlo calculation of the Fermi liquid parameters in the two-dimensional electron gas. *Phys. Rev. B* **50,** 1684–1694 (1994).
10. D'Amico, I. & Vignale, G. Spin diffusion in doped semiconductors: The role of Coulomb interactions. *Europhys. Lett.* **55,** 566–572 (2001).
11. Kato, Y. K., Myers, R. C., Gossard, A. C. & Awschalom, D. D. Observation of the spin Hall effect in semiconductors. *Science* **306,** 1910–1913 (2004).
12. Wunderlich, J., Kaestner, B., Sinova, J. & Jungwirth, T. Experimental observation of the spin Hall effect in a two-dimensional spin-orbit coupled semiconductor system. *Phys. Rev. Lett.* **94,** 047204 (2005).
13. Flensberg, K., Jensen, T. S. & Mortensen, N. A. Diffusion equation and spin drag in spin-polarized transport. *Phys. Rev. B* **64,** 245308 (2001).
14. D'Amico, I. & Vignale, G. Spin Coulomb drag in the two-dimensional electron liquid. *Phys. Rev. B* **68,** 045307 (2003).
15. Kikkawa, J. M. & Awschalom, D. D. Lateral drag of spin coherence in gallium arsenide. *Nature* **397,** 139–141 (1999).
16. Vohringer, P. & Scherer, N. F. Transient grating optical heterodyne detected impulsive stimulated Raman-scattering in simple liquids. *J. Phys. Chem.* **99,** 2684–2695 (1995).
17. Chang, Y. J., Cong, P. & Simon, J. D. Optical heterodyne-detection of impulsive stimulated Raman-scattering in liquids. *J. Phys. Chem.* **99,** 7857–7859 (1995).
18. Gedik, N. & Orenstein, J. Absolute phase measurement in heterodyne detection of transient gratings. *Opt. Lett.* **29,** 2109–2111 (2004).

Supplementary Information is linked to the online version of the paper at www.nature.com/nature.

Acknowledgements We thank I. D'Amico and G. Vignale for sending us numerical evaluations of their integral expression for the spin drag resistance. This work was funded by the US DOE, DARPA, and NSFDMR. We also acknowledge support from the Fannie and John Hertz Foundation (C.P.W.) and the Hellman Foundation (J.E.M.).

Author Information Reprints and permissions information is available at npg.nature.com/reprintsandpermissions. The authors declare no competing financial interests. Correspondence and requests for materials should be addressed to C.P.W. (cpweber@lbl.gov).